Microelectronics Reliability 55 (2015) 1067–1076

Contents lists available at ScienceDirect

Microelectronics Reliability

journal homepage: www.elsevier.com/locate/microrel

Improving cooling effectiveness by use of chamfers on the top of electronic components

Nemdili Saleha, Nemdili Fadèla, Azzi Abbès *

Laboratoire Aero-Hydrodynamique Navale, LAHN, USTO-MB University, BP1505 El-Mnaouar, 31000 Oran, Algeria

ARTICLE INFO

Article history:
Received 3 November 2014
Received in revised form 27 February 2015
Accepted 17 April 2015
Available online 27 April 2015

Keywords:
Electronic component
Cooling effectiveness
Wall mounted cube
Impinging jet
Shear Stress Transport (SST) turbulence model
Jet in cross flow

ABSTRACT

A Computational Fluid Dynamic (CFD) study based on Reynolds Averaged Navier–Stokes (RANS) approach is carried out to predict the mean velocity field and the heat transfer rate of an impinging jet in cross-flow configuration on a heated wall-mounted cube. Targeting an electronic cooling configuration, the aim is to investigate the effect of geometrical modification of the component on the cooling effectiveness. For the same cross flow Reynolds number $Re_H = 3410$, three levels of impinging jets are computed as well as a case without impinging jet that will serve as baseline case for comparison. The results from the RANS computation are compared to experimental data from published scientific literature. The validation shows qualitatively good agreement and almost all flow structures are well reproduced by the computation. In an attempt to optimize the wall heat flux over the cube surface, a new geometry is proposed without sharp corners on the top cube face. Numerical results show that with minor geometrical modification (chamfer), the fluid flow structure around the electronic component is radically transformed and the heat transfer rate can be improved. The highest cooling effectiveness improvement is realize for the highest Reynolds number ratio $Re_j/Re_H = 1.5$ and for the chamfer height of 4 mm.

1. Introduction

In electronics industry overheating is the main cause of failure and the major limitation to further increase in the power and efficiency. Taking into account the Moore's law [1] that states: the power of each new generation of microprocessor doubles, one can understand that intensive cooling of electronic components is more than necessary. A good and efficient cooling design is an uncounturnable condition to reliable long-term operation in electronic applications. In this context, general problems of microelectronic reliability are discussed by White and Bernstein [2], while the specific problem of high temperature is addressed by Petch [3]. In a very detailed report, Petch [3] attempts to address important questions related to microelectronic device design, cooling system, weight and reliability. According to the definition of reliability, it is shown that high temperature can cause equipment failure but can also affect the normal performance requirements. Especially that in real life, the operating conditions cannot be only in steady-state regime but can be also cyclic, with gradient and time-dependent. All this aspects and much more are presented and discussed in the report [3]. One example of the temperature effects is highlighted by Li et al. [4] who showed that in the case of the high-power light-emitting diodes (LEDs) when the temperature increases by 1 °C, luminescence intensity decreases by 1% and wavelength of light-wave changes 0.2–0.3 nm which leads to the changes of light color. If the heat cannot dissipate properly, it will lead excessive temperature, shorten the life, and thermal stress will damage the LEDs chip.

Forced channel air flow is the most frequently solution used for cooling Printed Circuit Board (PCB), see Meinders [5]. It is important to find the optimal ways to dissipate the maximum heat from electronic components while maintain energy consummation and noise level at their minimum possible values. One of the most relevant and cited study in this field is that done by Tummers et al. [6], who conducted an experimental investigation using an in-line array of five cubes, where detailed particle-image velocimetry (PIV) and infrared thermography measurements were reported.

Additionally to the experimental investigations, Computational fluid Dynamic (CFD) is an economic alternative to predict and test several geometrical and thermal configurations in order to optimize the cooling in terms of size, blowing power and avoiding local hot spots. One possible geometrical configuration that can mimics a realistic electronics cooling is the wall mounted cube and in some cases an in-line row of several cubes mounted on the lower wall in a plane channel flow.

* Corresponding author.
E-mail address: azzi.abbes@yahoo.fr (A. Abbès).

http://dx.doi.org/10.1016/j.microrel.2015.04.006
0026-2714/

In an earlier experimental study conducted by Martinuzzi and Tropea [7], the flow around surface-mounted prismatic obstacles with different spanwise dimensions is investigated. The main aim of their research is first to add experimental data related to the complex flow filed for this configuration to the Journal of Fluids Engineering Data Bank and also to find the geometrical limit between nominally two-dimensional and fully three-dimensional obstacle flows. They found that the middle region of the wake is nominally two-dimensional for width to height ratios (W/H) greater than 6. They also highlight the complex flow around a surface-mounted cube by the much known schematic representation that was reproduced by several researchers and reported here in Fig. 6(a).

In addition to the general problem of removing highly concentrated heat, the local hot spots can cause local overheating and thermal fatigue. This is a specific critical problem that has to be considered by electronic devices designers. In case of using only a forced channel flow, excessive flow rates will be required. One possible method to face this problem is to use the high heat removal rates of impinging jets to enhance and optimize the cooling design. So as explained by Rundström and Moshfegh [8,9], in addition to the channel flow, impinging jets are used separately for the most dissipating component.

A numerical investigation of fluid flow and heat transfer characteristics associated with cooling in-line array of discrete heated blocks in a channel by using single laminar air jet has been recently presented by Arquis et al. [10]. In addition to different values of jet Reynolds number, they conducted many tests for different geometrical parameters. They found that effective cooling of blocks is proportionally related to the Reynolds number and inversely proportional to the channel height. Heat transfer rates are also found to be enhanced for shorter and widely spaced heated blocks. As natural finding, the block just underneath the impinging air jet is found to be the most cooled one. The values of surface averaged Nusselt number decrease for downstream blocks, and approximately reach a constant value after the third block. In their discussion, Arquis et al. [10] highlight the close relationship between the circulation bubbles on the top surface of blocks and the low values of Nusselt numbers.

Reynolds Averaged Navier–Stokes (RANS) calculations of the flow and heat transfer for flow over a heated, jet-impinged, wall-mounted cube in a cross-flow have been reported by Rundström and Moshfegh [11], while Popovac and Hanjalic [12] report Large Eddy Simulation for nearly similar configuration. Both simulations attempt to represent a simplified case of electronics cooling. The targeted cube is cooled by two mutually perpendicular streams of air: a channel air at $Re = 4800$ and a round impinging jet $Re_j = 5200$. The study was aimed at investigating flow structures and turbulence statistics, as well as their thermal signature and heat transfer on the cube surface. The paper outlines the great capability of the Large Eddy simulation technic to validate at least qualitatively well against the experimental measurements.

One good example of CFD computation in this field is the study conducted by Octavio et al. [13], who studied numerically the effect of aerodynamic shaping of the cooling fins in staggered heat sinks. They show that by rounding the cooling fins, the aerodynamic efficiency is increased without affecting the thermal efficiency. By comparing three different geometries, they found that a rounded staggered fin layout can remove the same heat as a classical in-line fin layout with a reduction of fan power consumption by more than 60%.

In the same strategy, the present study aims to show that with some geometrical modifications of the cube corners, the thermal efficiency can be improved when keeping the same amount of cold blowing.

In the present study, it is focused on a single wall mounted cube cooled simultaneously by a jet in a cross flow. This configuration is nearly identical to that studied experimentally by Masip et al. [14] in which a set of three main Reynolds numbers combined with three ratios are considered. The combination of the two parameters results in nine different data series. In the present study the validation is limited to the first three cases corresponding to the main Reynolds number of 3410 and three Reynolds number ratios. The main Reynolds number is based on the channel bulk velocity ($U_{inf} = 1.705$ m/s) and the channel height ($H = 2h$). The three ratios (Re_j/Re_H) considered are 0.5, 1.0 and 1.5 which correspond to three $Re_j = 1705$, 3410 and 5115 respectively. The jet Reynolds numbers (Re_j) are computed based on their bulk velocity U_j and the diameter

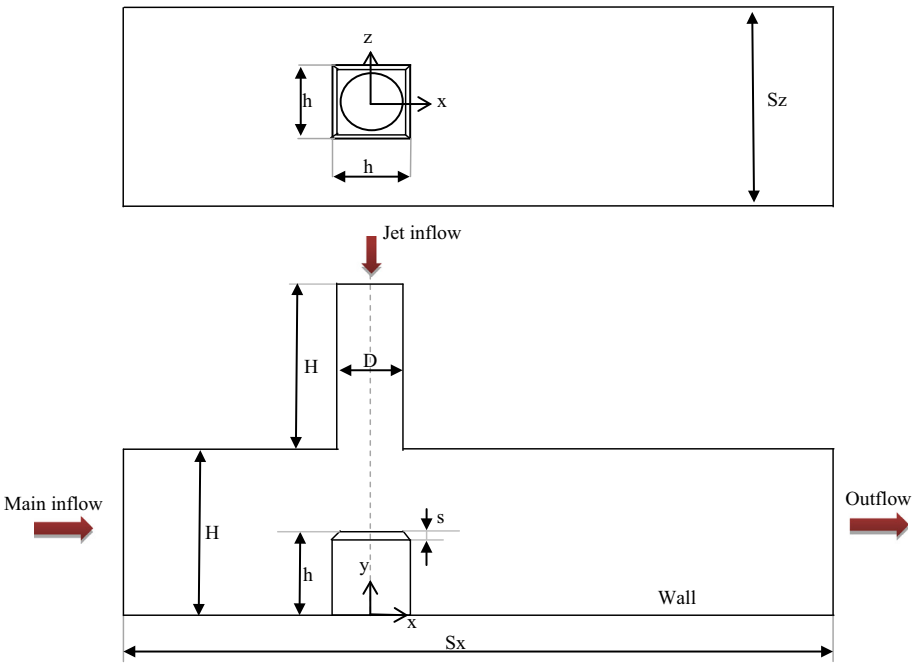

Fig. 1. Computational domain, boundary conditions and local coordinate system.

of the orifice D. A fourth case without the impinging jet is also computed for comparison purpose and referred as baseline case. In an attempt to enhance the heat transfer over the cube, a modified geometry is proposed, where the top corners are modified in such a way to avoid the sharpness by adding local chamfers. The cases will be noted hereafter as follow: F00, F05, F10 and F15 for baseline case, $Re_j/Re_H = 0.5$, 1.0 and 1.5 respectively. Combining the Reynolds number ratio ($Re_j/Re_H = 1.5$) and chamfer heights three additional cases are computed. They will be noted FC115, FC215 and FC315 for chamfer heights of 1, 2 and 4 mm respectively.

2. Flow configuration and computational details

As mentioned before, geometrical details and computational parameters are similar to those in the experimental work of Masip et al. [14]. So, the computational domain is a rectangular channel with a cube ($h = 15$ mm) in the middle of the bottom wall. The channel has two inlets; one horizontal channel flow and one vertical round impinging jet (see Fig. 1). The impinging jet has a diameter of 12 mm. The cube and the cylindrical hole are centered with geometrical axis as shown in Fig. 1, where the X-axis, Y-axis and Z-axis refer to the streamwise, the normal and the spanwise directions, respectively. In order to get realistic boundary conditions for the jet when leaving the hole, a cylindrical conduit of 30 mm long is added to the computational domain. The geometrical details, properties and boundary conditions are summarized in Table 1, while Table 2 shows the seven test cases considered in the present study.

Table 1
Geometric and flow details.

Jet diameter	D	12 mm
Component height	h	15 mm
Channel height	H	$2h = 30$ mm
Chamfer height	s	1, 2 and 4 mm
Channel bulk velocity	U_{inf}	1.705 m/s
Computational domain length	S_x	1000 mm
Computational domain width	S_z	150 mm
Reynolds number based on the channel height and channel bulk velocity	Re_H	3410

Table 2
Details of computed cases.

	Chamfer heights	Re_j/Re_H	Re_j	U_j (m/s)
Case 1, F00	Regular cube	0.0	0.0	0.0
Case 2, F05		0.5	1705	2.131
Case 3, F10		1.0	3410	4.262
Case 4, F15		1.5	5115	6.393
Case 5, FC115	1 mm	1.5	5115	6.393
Case 6, FC215	2 mm	1.5	5115	6.393
Case 7, FC315	4 mm	1.5	5115	6.393

3. Numerical details

The present simulations were conducted using the ANSYS-CFX package, where the solution of the Reynolds Averaged Navier–Stokes (RANS) and energy equations is obtained using the finite

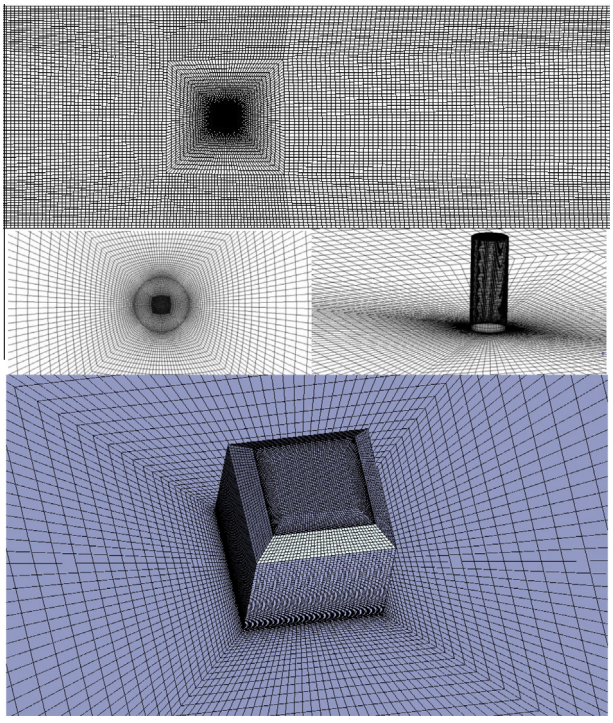

Fig. 3. Computational mesh.

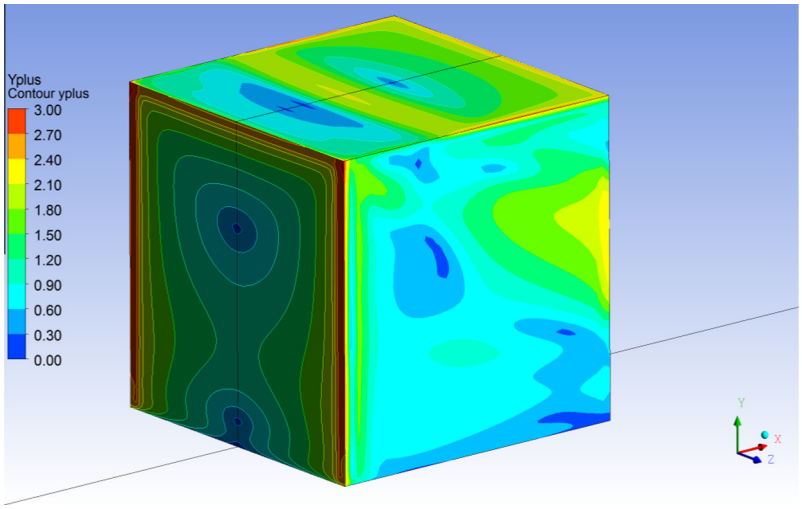

Fig. 2. y^+ values at one cell above the surface of solid walls (case F05).

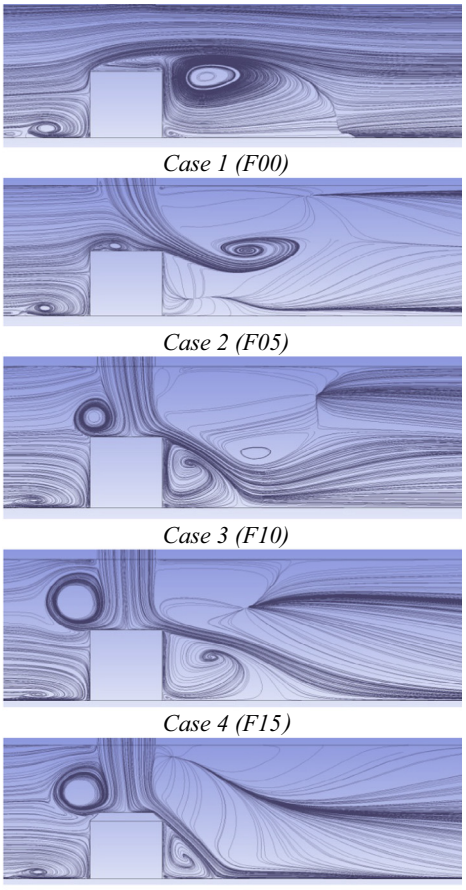

(a) Present computation

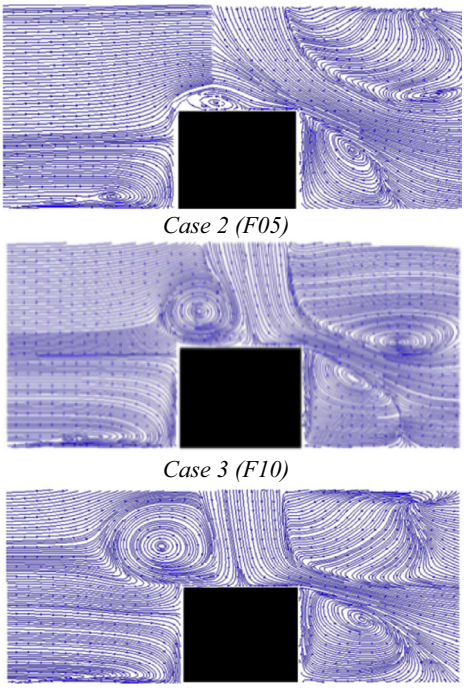

(b) Experiment from [6]

Fig. 4. Streamlines in the *XY* plane at $z/h = 0$ for $Re_H = 3410$.

volume method with a body-fitted hexahedral unstructured grid. A co-located layout is employed in which the pressure, turbulence, and velocity unknowns share the same location. The momentum and continuity equations are coupled through a pressure correction scheme, and several implicit first- and second-order accurate schemes are implemented for the space and time discretizations. In the present computation, convection terms are discretized with a second order scheme except near discontinuities, where it reduces to first order to preserve boundedness. The turbulence closure is achieved by use of the well-known Shear Stress Transport (SST) $k-\omega$ based model proposed by Menter [15]. This model is known to provide a good compromise by combining the $k-\omega$ model of Wilcox in the near the wall region and the high Reynolds $k-\varepsilon$ model in the outer region. The use of the two models is realized via a blending function, which switches from one to zero depending on the geometrical position of the integration point. Detailed explanation of the model formulation and test case validations can be found in specific literature of Menter's group [15], while only the mathematical equations of the model are presented here.

To build the SST model, the Wilcox model is multiplied by a blending function F_1 and a transformed version of the $k-\varepsilon$ model

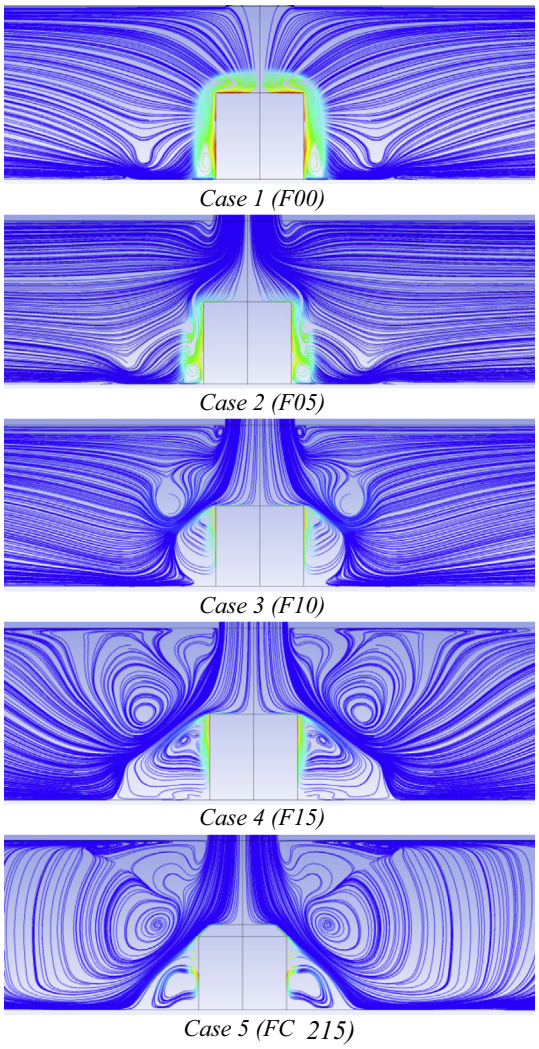

Fig. 5. Streamlines in the *YZ* plane at $x/h = 0$ for $Re_H = 3410$, colored by the temperature.

by a function $(1 - F_1)$. F_1 is equal to one near the solid walls and decreases to a value of zero outside the boundary layer. At the boundary layer edge and outside the boundary layer, the standard $k - \varepsilon$ model is therefore recovered. Then the corresponding k and ω equations are added to give the new model formula given by Eqs. (1) and (2).

$$\frac{\partial(\rho k)}{\partial t} + \frac{\partial(\rho U_j k)}{\partial x_j} = \frac{\partial}{\partial x_j}\left[\left(\mu + \frac{\mu_t}{\sigma_{k3}}\right)\frac{\partial k}{\partial x_j}\right] + P_k - \beta^* \rho k\omega + P_{kb} \quad (1)$$

$$\frac{\partial(\rho\omega)}{\partial t} + \frac{\partial(\rho U_j \omega)}{\partial x_j} = \frac{\partial}{\partial x_j}\left[\left(\mu + \frac{\mu_t}{\sigma_{\omega 3}}\right)\frac{\partial \omega}{\partial x_j}\right] + (1 - F_1)2\rho\frac{1}{\sigma_{\omega 2}\omega} \times \frac{\partial k}{\partial x_j}\frac{\partial \omega}{\partial x_j} + \alpha_3 \frac{\omega}{k} P_k - \beta_3 \rho\omega^2 \quad (2)$$

The coefficients of the new model are a linear combination of the corresponding coefficients of the two previous models:

$$\varphi = F_1\varphi_1 + (1 - F_1)\varphi_2 \quad (3)$$

All coefficients are listed here:

$$\beta^* = 0.09, \quad \alpha_1 = 5/9, \quad \beta_1 = 0.075, \quad \sigma_{k1} = 2, \quad \sigma_{\omega 1} = 2,$$
$$\alpha_2 = 0.44, \quad \beta_2 = 0.0828, \quad \sigma_{k2} = 1 \text{ and } \sigma_{\omega 2} = 1/0.856$$

In order to avoid the known over-prediction of the eddy-viscosity linked with original $k - \omega$ model, the SST model uses a limiter to the formulation of the eddy-viscosity given by Eq. (4).

$$\nu_t = \frac{a_1 k}{\max(a_1\omega, SF_2)} \quad (4)$$

$$\nu_t = \mu_t/\rho \quad (5)$$

Again F_2 is a blending function similar to F_1, which restricts the limiter to the wall boundary layer and S is an invariant measure of the strain rate. The blending functions F_1 and F_2 are critical to the success of the method. Their formulation is based on both the distance to the nearest surface and on the flow variables (see Menter [15] for more discussion on this point).

After many tests and according to the best compromise between precision and available computational facilities a grid of about two million structured hexahedral cells was adopted for all cases. The grid was checked at posteriori by plotting the y^+ contours which is maintained less than unity for the first grid point away from all viscous walls. This is true for approximately all points with some exception where y^+ can reach the value of three. With this condition the viscous sublayer near solid walls, which extend until $y^+ = 5$, can be properly resolved. The grid points are also well stretched near the walls and in the vicinity of the cube. Fig. 2, shows the y^+ contours on the wall, while the computational grid is highlighted by Fig. 3.

The following boundary conditions are used (see Fig. 1): the top boundary including inside the hole injection, the bottom walls including the cube and the side walls have no-slip conditions. The outflow conditions are set to zero-gradient condition and finally the same temperature 20 °C is used for the channel flow and the impinging jet. All walls boundaries are maintained at constant temperature, 60 °C for the cube and 20 °C for the remaining walls.

4. Results and discussion

Fig. 4 represents streamlines in the XY plane at $z/h = 0$ for all computational cases as well as the experimental one from Masip et al. [14]. Globally and compared to experimental figures, the main

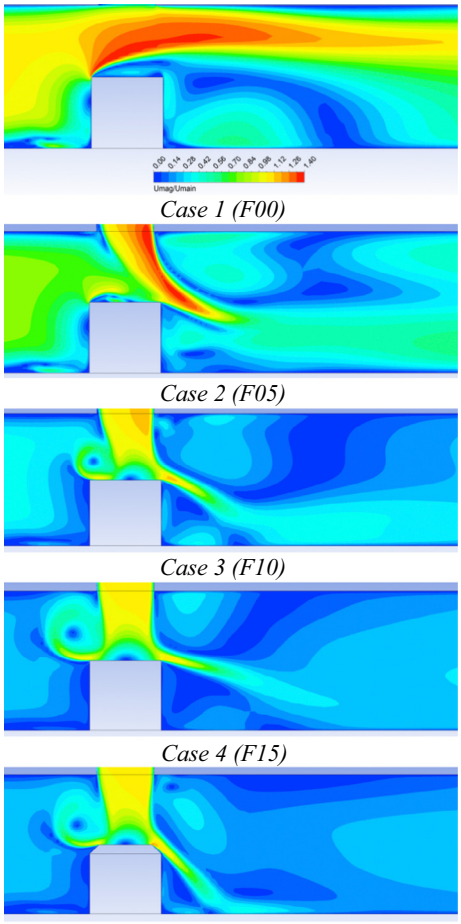

Fig. 6. Contours of V_{mag}/U_j in the XY plane at $z/h = 0$ for $Re_H = 3410$.

features of flow configuration are well reproduced by the present RANS simulation. For the low Reynolds number ratio (0.5), the jet is strongly deviated into the downstream direction, while for medium Reynolds number ratio (1.0) the jet impinges on the top cube surface. In the case of the high Reynolds number ratio (1.5) the jet also impinges the top cube surface and additionally there is a small part of it that sweeps along the cube front face. As reported by previous investigations this part of jet sweeping along the cube front face can improve considerably the cooling of the cube. In a preliminary experiment of Flikweert [16], he showed that the maximum cooling effect of the cube was achieved when the jet axis was moved upstream from the cube center by a small distance. This position increases the part of the impingement jet that sweeps along the front face. When looking at the modified geometry (with chamfers), one can see that without the sharp corner, more cooling flows are sweeping along the cube rear face. So, at the front face the flow retrieve the first configuration corresponding to the lowest ratio. This configuration is characterized by a recirculation bubble that develops and goes smaller and moves in the upstream direction when the Reynolds number ratio increases. For the last modified case (FC215) the bubble has the same size and the same place of the first case. This can be explained by the fact that more cooling jet flow is deviated to the rear cube face. This situation is more helpful to the cooling process since the front face is mainly cooled by the main flow itself and rear face needs to be more considered by the jet flow. One can also identify for the lowest Reynolds number ratio, a separation and reattachment region on the top cube surface. This recirculation zone disappears when the Reynolds number ratio goes higher.

Fig. 5 shows the streamline in *YZ* plane at $x/h = 0$. The streamlines are colored by the temperature and highlight clearly the bubbles at the side faces of the cube. The jet flow decelerates at the top of the cube and then turns sharply to form a radial wall jet. At the corner, the flow separates and reattaches downstream creating a recirculation bubble that has important effect on the wall heat flux. The last case without sharp corners (FC215) shows that the impinging cold jet swept closely to the side faces when compared to the previous case (F15).

Additional comparison is highlighted by Fig. 6 showing the contours of the mean velocity magnitude adimensionalized by the impinging jet velocity except for the F00 case which it is adimensionalized by the main channel velocity. The same phenomenology described and discussed in the previous figure (Fig. 4) is confirmed here. As said before for the lowest Reynolds number ratio the jet is dragged by the channel flow and does not reach the top face of the cube, while there is a visible jet impingement growing proportionally to the Reynolds number ratio.

For the modified case (FC215), the recirculation bubble downstream the cube became smaller and is replaced by a benefic sweeping cold jet.

As the configuration of flow in a surface-mounted obstacle is very complex and is of great academic and application interest,

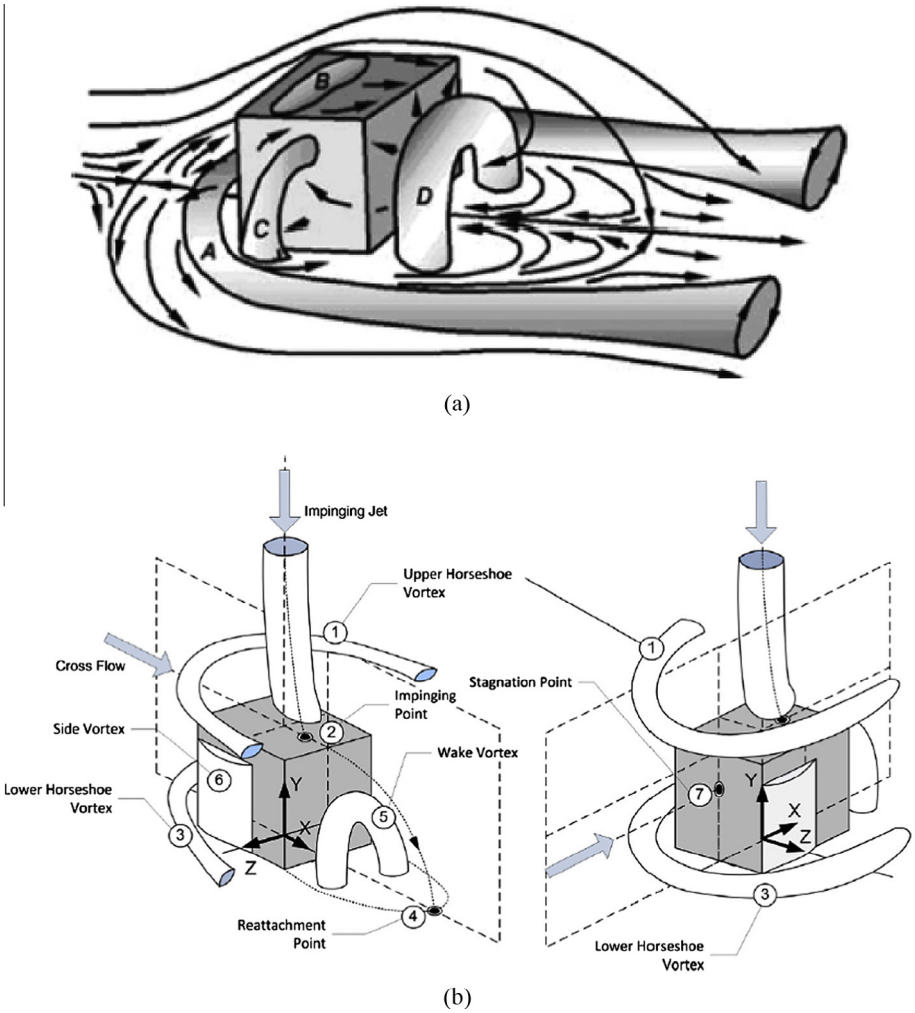

Fig. 7. (a) Mean flow structures around a wall mounted cube [7]. (b) Mean flow structures around a cube cooled by an impinging jet in a cross flow [14].

many researchers [7,14] worked to highlight the morphology of the nearest flow as showed at Fig. 7. The two sketches correspond to cube without and with impingement jet respectively and highlight the main vortices accompanying this configuration. In Fig. 8 an attempt to highlight the morphology of the flow is done by use of iso-surfaces of the so-called *Q*-criteria, function of vorticity and strain rate of the flow field. Iso-surfaces are colored by the velocity magnitude.

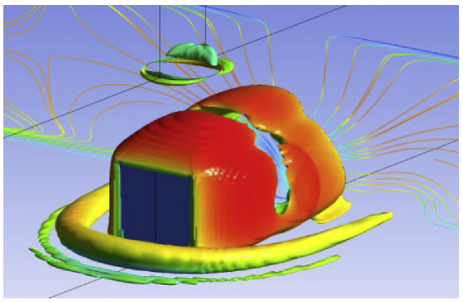

Case 1 (F00)

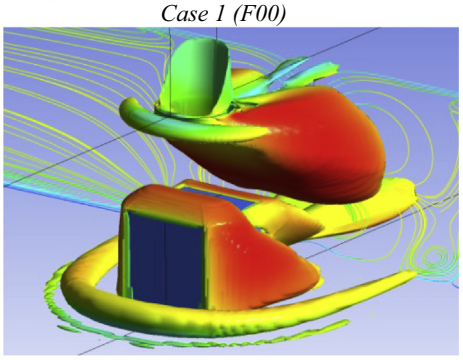

Case 2 (F05)

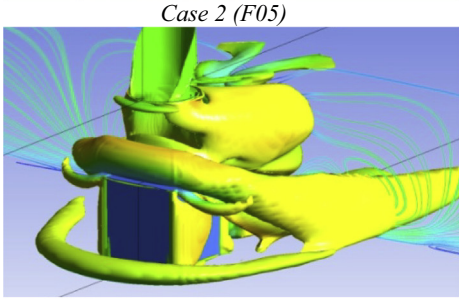

Case 3 (F10)

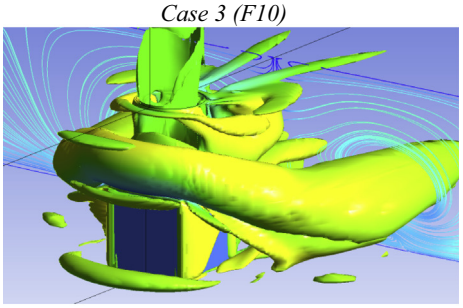

Case 4 (F15)

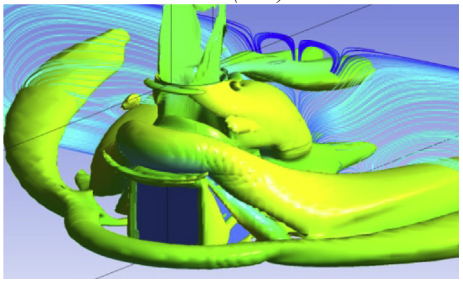

Case 5 (FC215)

Fig. 8. Isosurfaces of the so-called *Q*-criteria (6000 (s^{-2})) colored by the longitudinal velocity.

The horseshow vortex in front of the cube is well reproduced for the baseline case, as well as the upper horseshow vortex developing around the jet. This vortex is rapidly growing with Reynolds number ratio and becoming more complex and deviates down for the last modified case (FC215).

Before moving to the heat transfer fields, Fig. 10 represents a quantitative comparison of longitudinal velocity at several locations before and after the cube. The exact locations are highlighted by Fig. 9 and are as follow: one line in front of the cube (Line1 $x/H = -0.75$), one line on top of the cube (Line2, $x/H = 0.0$) and two lines downstream of the cube in the recirculation zone ($x/H = 1$ and 1.5). Globally, the longitudinal velocity profiles agree reasonably with the experimental ones in almost all locations. Some differences are reported in some profiles parts and can be attributed mainly to differences in inlet boundary conditions and also to the limitations of the turbulence modeling strategy adopted in frame of RANS approach. Nevertheless, the global behavior and qualitative results are reproduced in a satisfied level taking into account the numerically economic strategy adopted.

The three Reynolds numbers ratios as well as the base line case are presented. At the first location, one can see for the first case (baseline case) the slightly modified channel velocity profile. The profile is characterized by a decreasing velocity in the lowest half of the channel and an accelerating behavior in the top half. This is due mainly by the presence of the cube as an obstacle in the bottom part of the channel. This trend is conserved for the lowest Reynolds number ratio (0.5) but radically modified for the two remaining cases. As an effect of the jet penetration, the longitudinal velocity decreases even in the top half of the channel and for the highest Reynolds number ratio, one can see that the flow goes in negative direction in the middle of the channel. The present RANS computation agrees well the experiment measurements at the lower part of the channel, where it shows some underestimation of the reverse flow in the middle (see the first panels in Fig. 10).

When looking at the second location, which is located exactly on the middle top of the cube, the base line case is characterized by a normal channel profile with a small reverse flow near the top face of the cube. This reverse flow corresponds to the detached and reattached boundary layer on the top of the cube. This behavior is well predicted by the model especially the reverse flow for case 3. Nevertheless, the highest Reynolds number ratio case (case 4) is worthy reproduced and the reverse flow seems to be completely ignored by the computation. This can be expected, since the two equation turbulence model is well known to reproduces poorly the stagnation regions.

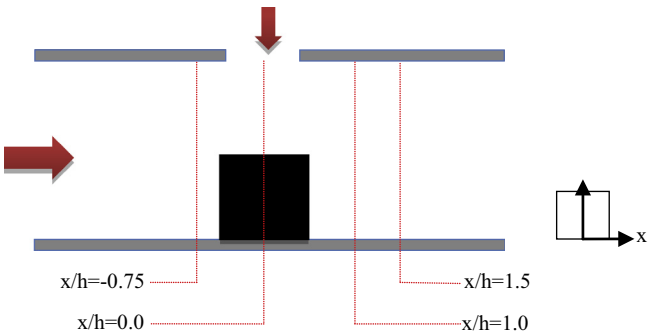

Fig. 9. Selected vertical lines where results are compared to experimental data.

The next locations (x/H = 1 and 1.5) highlights the jet deviation and penetration in the middle of the channel. The qualitative experimental behavior is satisfactory reproduced by the numerical model, while quantitatively some discrepancies can be reported. The vertical jet, after impinging the cube, goes in horizontal direction with a sensible acceleration in the middle of the channel. Note

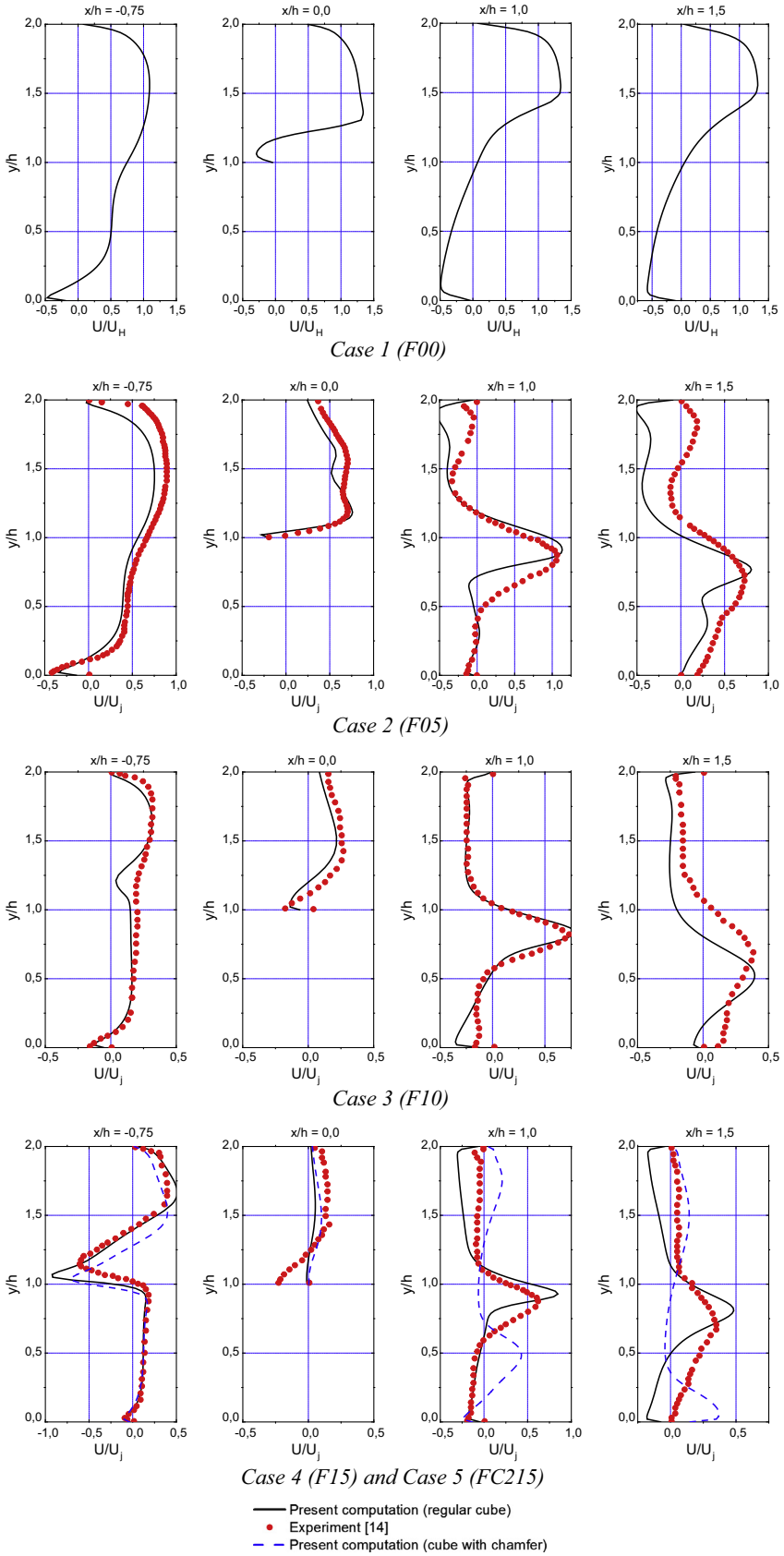

Fig. 10. U velocity profiles $z/h = 0$ for $Re_H = 3410$.

that for the modified case (case FC215) and due to the chamfer the jet is deviated toward the bottom wall, which is well predicted by the numerical model.

Contours of temperature on the central plan ($z/H = 0$) are presented in Fig. 11. As expected by previous results, the thickness of the thermal boundary layer decreases when increasing the Reynolds number ratio and the thermal shape follows the flow vortices. The wall heat flux at the surface of the cube is presented at Fig. 12 in a front view. At the front face, the contours have slightly the same behavior, while at the top and side faces the impinging jet power modifies and increases the wall heat distribution. The last modified case shows the highest levels of wall heat flux.

When comparing the turbulent vortex structures near the cube (Fig. 8) to the temperature field (Figs. 11 and 12), a significant correlation is found between the two. The turbulent vortex structures at the separations from the edges carried a large amount of heat. This is clearly highlighted by the yellow color (high values of heat flux) on the front edges. For the modified case, which is the more cooled one, yellow color can be seen on the top region edge.

Finally, the amount of wall heat flux exchanged by each side and the global heat flux are presented at Fig. 13. The figure shows

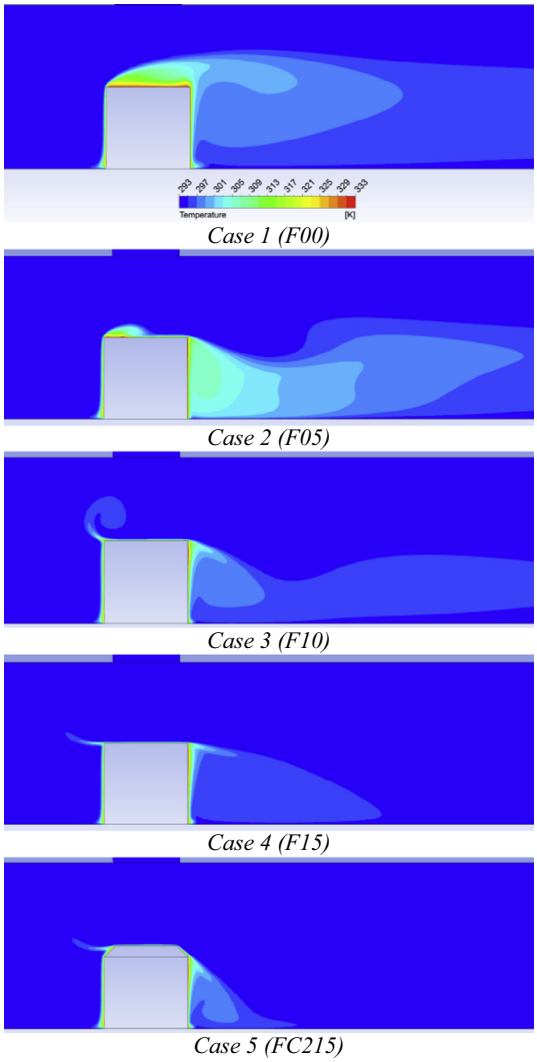

Case 1 (F00)

Case 2 (F05)

Case 3 (F10)

Case 4 (F15)

Case 5 (FC215)

Fig. 11. Temperature contours at $z/h = 0$ for $Re_H = 3410$.

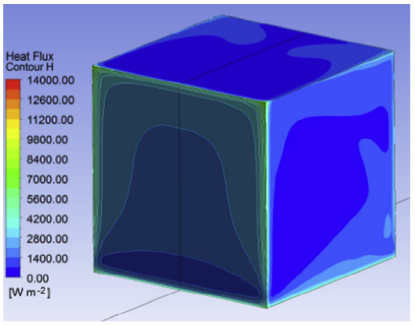

Case 1 (F00)

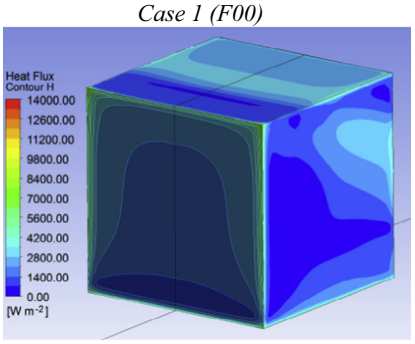

Case 2 (F05)

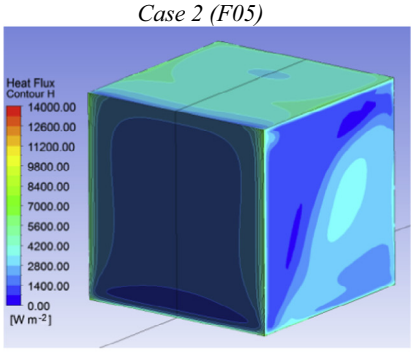

Case 3 (F10)

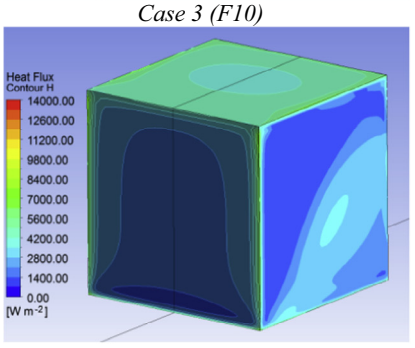

Case 4 (F15)

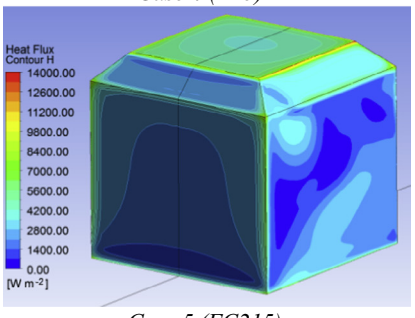

Case 5 (FC215)

Fig. 12. Contours of heat flux density on the surface of the cube, front view.

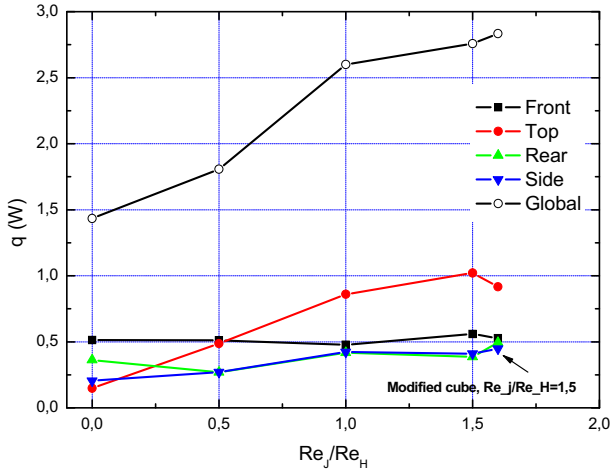

Fig. 13. Total heat flux on the global surface of the cube and by face.

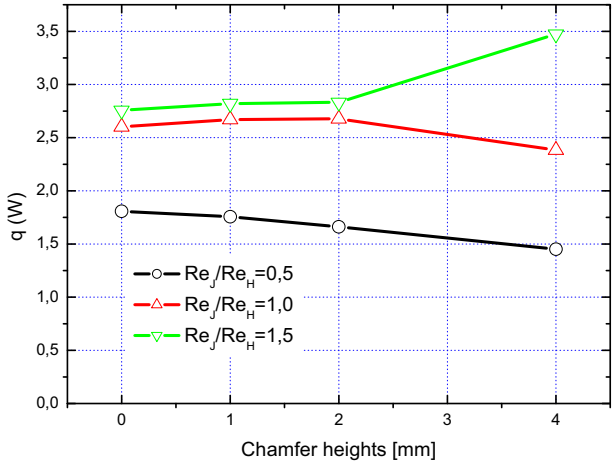

Fig. 14. Total heat flux on the global surface of the cube versus chamfer heights.

that the wall heat flux at the front face is always the same for all configurations. It increases at side walls until ($Re_j/Re_H = 1.0$) and then remains constant. At rear side, it decreases from ($Re_j/Re_H = 0.0$) to ($Re_j/Re_H = 0.5$) and follows the behavior of the side faces. At the top face, the wall heat flux increases significantly when the impinging jet velocity increases. The modified geometry proposed shows some amelioration at rear and side faces while it remains the same for the front face. The smaller wall heat flux at the top face of the FC215 case can be related to the decreases in face area when applying the geometrical modification. When looking at the global wall heat flux for the cube, it increases proportionally to the Reynolds number ratio with moderate amelioration when comparing the FC215 case to the F015.

In order to study the effect of the chamfer height on the cooling effectiveness, three values of the chamfer height are tested. They are 1, 2 and 4 mm corresponding to FC115, FC215 and FC315 respectively. The global heat flux for the three cases as well as for the regular cube (F15) is represented by Fig. 14. As we can see, for the two lowest Reynolds number ratio ($Re_j/Re_H = 0.5$ and 1.0) the chamfer does not add any improvement to the cooling effectiveness. It remains constant for $Re_j/Re_H = 1.0$ and $0 < s < 2$ and then it decreases for $s = 4$ mm, while it decreases monotonically for $Re_j/Re_H = 0.5$. In contrast, for the highest Reynolds number ratio $Re_j/Re_H = 1.5$, the chamfer gives some (3%) cooling improvement for $s = 1$ and 2 mm and absolutely a better (26%) cooling effectiveness for $s = 4$ mm.

5. Conclusions

The predictions of the mean velocity and the thermal field of an impinging turbulent jet in cross-flow configuration over a heated wall-mounted cube are carried out. The numerical approach adopted here is based on the well-known two equations turbulence model called Shear Stress Transport (SST) model. Despite the moderate demand in computer resources compared to other direct simulation strategies, the study gives a good tool to reproduce the main features of this configuration including the optimization and the selection between many variants. Increasing the Reynolds number ratio until the value of 1.0 can improve considerably the wall heat transfer. After this value, the gain will be moderate, which suggests for economic reason to keep the ratio at value of 1.0. It was found also that a small geometrical modification on the top cube face can increase the global wall heat flux and add some effectiveness to the cooling process. The computational results show that the gain can be realized only for the highest Reynolds number ratio ($Re_j/Re_H = 1.5$) and it is better for last case which correspond to a chamfer height of 4 mm.

References

[1] Moore G. Cramming more components into integrated circuits. Electron Mag 1965;38:114–7.
[2] White Mark, Bernstein Joseph B. Microelectronics reliability: physics-of-failure based modeling and lifetime evaluation. Jet Propulsion Laboratory California Institute of Technology Pasadena, California, JPL Publication 08-5 2/08, <http://nepp.nasa.gov>.
[3] Pecht Michael. The influence of temperature on microelectronic device failure, US Army SBIR PHASE II, final report, Ramsearch Company, Crofton; September 4, 1993.
[4] Li J, Bangke Ma, Wang R, Han L. Study on a cooling system based on thermoelectric cooler for thermal management of high-power LEDs. Microelectron Reliab 2011;51:2210–5.
[5] Meinders ER. Experimental study of heat transfer in turbulent flows over wall-mounted cubes. Ph.D. Thesis. Delft University of Technology, The Netherlands; 1998.
[6] Tummers MJ, Flikweert MA, Hanjalić K, Rodink R, Moshfegh B. Impinging jet cooling of wall-mounted cubes. In: Proceedings of ERCOFTAC, international symposium on engineering turbulence modelling and experiments – ETMM6, Sardinia, Italy; 2005. p. 773–91.
[7] Martinuzzi RJ, Tropea C. The flow around surface mounted, prismatic obstacles placed in a fully developed channel flow. J Fluids Eng 1993;115:85–92.
[8] Rundström D, Moshfegh B. Investigation of flow and heat transfer of an impinging jet in a cross-flow for cooling of a heated cube. ASME J Electron Pack 2006;128:150–6.
[9] Rundström D, Moshfegh B. Large-eddy simulation of an impinging jet in a cross-flow on a heated wall-mounted cube. Int J Heat Mass Transf 2009;52:921–31.
[10] Arquis E, Rady MA, Nada SA. A numerical investigation and parametric study of cooling an array of multiple protruding heat sources by a laminar slot air jet. Int J Heat Fluid Flow 2007;28:787–805.
[11] Rundström D, Moshfegh B, Ooi A. Rsm and v2-f predictions of an impinging jet in a cross flow on a heated surface and on pedestral. In: 16th Australasian fluid mechanics conference crown plaza, 2–7 December 2007, Gold Coast, Australia; 2007.
[12] Popovac M, Hanjalic K. Large-eddy simulations of flow over a jet-impinged wall-mounted cube in a cross stream. Int J Heat Fluid Flow 2007;28:1360–78.
[13] Leon Octavio A, De Mey Gilbert, Dick Erik, Vierendeels Jan. Staggered heat sinks with aerodynamic cooling fins. Microelectron Reliab 2004;44:1181–7.
[14] Masip Yunesky, Rivas Alejandro, Larraona Gorka S, Anton Raúl, Ramos Juan Carlos, Moshfegh Bahram. Experimental study of the turbulent flow around a single wall-mounted cube exposed to a cross-flow and an impinging jet. Int J Heat Fluid Flow 2012;38:50–71.
[15] Menter FR. Zonal two-equation k–eps turbulence model for aerodynamic flows. AIAA Paper 1993:93–2906.
[16] Flikweert M. Flow and heat transfer investigation of wall-mounted cubes in cross-flow. M.Sc. thesis. Delft University of Technology, Delft, The Netherlands; 2005.